applied optics

Evaluating an image-based bidirectional reflectance distribution function measurement setup

Aditya Sole,[1,*] Ivar Farup,[1] Peter Nussbaum,[1] and Shoji Tominaga[1,2]

[1]The Norwegian Colour and Visual Computing Laboratory, Department of Computer Science, Faculty of Information Technology and Electrical Engineering, Norwegian University of Science and Technology, Gjøvik, Norway
[2]Department of Information Science, Graduate School of Engineering, Chiba University, Chiba, Japan
*Corresponding author: aditya.sole@ntnu.no

Received 27 September 2017; revised 30 January 2018; accepted 5 February 2018; posted 6 February 2018 (Doc. ID 307297); published 8 March 2018

We evaluate an image-based multiangle bidirectional reflectance distribution function measurement setup by comparing it to measurements from two commercially available goniospectrophotometers. The image-based setup uses an RGB camera to perform bidirectional measurements of the sample material. We use a conversion matrix to calculate luminance from the captured data. The matrix is calculated using camera spectral sensitivities that are measured with a monochromator. Radiance factor of the sample material is measured using a commercially available tabletop goniospectrophotometer and compared to measurements made using the image-based setup in the colorimetric domain. Our measurement setup is validated by comparing the measurements performed using a goniospectrophotometer. Uncertainty and error propagation is calculated and taken into account for validation. The sample material measured is wax-based ink printed on packaging paper substrate commonly used in the print and packaging industry. Results obtained show that the image-based setup can perform bidirectional reflectance measurements with a known uncertainty. The goniospectrophotometer measurements lie within the uncertainty of the measurements performed by the image-based measurement setup. The setup can be used to perform bidirectional reflectance measurements on samples with properties similar to the samples used in this paper.

OCIS codes: (330.0330) Vision, color, and visual optics; (330.1710) Color, measurement.

https://doi.org/10.1364/AO.57.001918

1. INTRODUCTION

The quality of an object is often judged by its total appearance. To describe the physical correlates to the total appearance of an object (whether it is food, textile, skin, chemicals, coatings, metals, paper, or plastics) optical properties are measured. The overall appearance of an object/material results from a combination of its chromatic attributes (color described in terms of lightness, hue, and saturation) and its geometric attributes (like gloss, translucency, and texture) [1].

In recent years, various technologies (like effect inks [2] or conventional inks printed on metallic foils [3]) have been introduced particularly in the packaging industry to create appearance effects. These inks, however, cannot be described well enough by conventional measurements using a single measurement geometry.

For such materials the reflection of light is not satisfactorily modeled as, e.g., a Lambertian surface where the intensity of the light is proportional to the cosine of the reflection angle. They produce a desirable appearance by changing their perceived color or lightness properties with a change in illumination and viewing direction [4]. To characterize and reproduce such a material, reflectance measurements are performed at different illumination and viewing directions [4]. Back in 2007, Takagi *et al.* [5] stated that to characterize the reflection properties of special effect coatings, measurements taken at as many as 1485 different measurement geometries are required. It is practically very difficult to perform these measurements and use such huge data for processing. Kirchner and Cramer [6] demonstrated that a reduction in number of measurement geometries is essential and is possible with physical interpretation of the amount of light reflected at different measurement geometries. A recent study made by Ferrero *et al.* [7] to characterize the color shift of special effect coatings shows that a maximum of 10 geometries could be sufficient.

For traditional color pigments that are printed on diffuse paper substrates, traditional measurement geometries

recommended by CIE [8] are sufficient to characterize the materials in a way that correlates well with how the color of the material is perceived. In the graphic arts and print industry, measuring instruments with 45°:0° geometry are widely used for reflectance measurement of materials. Sphere-based geometries are mainly used in the paint, textile, and plastic industries. For nondiffuse materials like metallic inks the incident light is specularly reflected. ASTM standards [9,10] recommend the illumination and viewing directions for measurement of a few different types of the nondiffuse materials. Integrating sphere-based measurement instruments are often used to measure nondiffuse samples. However, using an integrating sphere-based instrument is not sufficient as it captures an average colorimetry of the sample and not the detailed angular variation of the reflected light. According to [4,11], using the traditional single geometry measurement instruments are also nonsufficient to measure and characterize such nondiffuse materials. Measurements made at more than one illumination and viewing directions are therefore required to characterize such materials.

Instruments measuring at a few selected multiple fixed directions are termed as a multiangle spectrophotometer [12], whereas instruments that are used for measurements over a broad range of angles are called goniospectrophotometers. In this paper, we adopt the terminology "goniospectrophotometer" to describe any instrument that performs measurements at more than one illumination and viewing direction.

A number of goniospectrophotometers are commercially available and widely used to perform measurements at different illumination and viewing directions [13]. These instruments measure the sample material spectrally at different illumination and viewing directions. The measurement quantity obtained is the ratio of the reflected and incident power ($\Phi_r/\Phi i$). Using this measurement quantity, the bidirectional reflectance distribution function (BRDF), f_r, of the material can be computed. Spectral radiant power and the corresponding radiometric terms required to express a BRDF are well defined and can be referred to in [14], and the BRDF is defined by Nicodemus *et al.* [15] as

$$f_r(\theta_i, \phi_i, \theta_r, \phi_r, \lambda) = \frac{dL_r(\theta_i, \phi_i, \theta_r, \phi_r, \lambda)}{dE_i(\theta_i, \phi_r, \lambda)}, \quad (1)$$

where $L_r(\theta_i, \phi_i, \theta_r, \phi_r, \lambda)$ is the reflected radiance in the direction (θ_r, ϕ_r), and $E_i(\theta_i, \phi_r, \lambda)$ is the irradiance from the direction (θ_i, ϕ_i). The illumination and viewing direction are described relative to the surface normal, so-called "anormal angle," in agreement with the ASTM E2175-01 [12] standard and the CIE 175 [16] technical report.

A goniospectrophotometer can measure at a broad number of illumination and viewing angles but are slow. One of the main reasons for this is that they require the sample material to be measured lying flat while the detector and the light source or the sample rotates to perform bidirectional measurements. The geometrical calibration for the detector and light source or sample surface rotation, and the spectral calibration of the incident light source contributes heavily to the measurement time of the instrument.

To overcome these drawbacks, image-based measurement setups have been proposed and presented in the past [17] to perform bidirectional measurements of flexible thin materials like print and packaging paper or plastic. Our setup used in this study can perform measurements fast (in a single shot) and in line with production of such print and packaging materials which can be an advantage over goniospectrophotometers. Guarnera *et al.* [18] provided an overview of measuring instruments that are used for bidirectional measurements.

Sole *et al.* [19,20] uses such a setup to measure thin flexible materials (printed packaging paper). The measured data is then used to train different reflection models (for example Cook–Torrance). In [21], Sole *et al.* trained two reflection models with measurement data captured using the image-based measurement setup described in [19,22]. One of the sample materials was also measured using a Minolta CS1000 telespectroradiometer (TSR) at four different viewing directions for a given illumination direction. Using the trained reflection models, the CIEXYZ Y value for the sample material was estimated at these four viewing directions for the given illumination direction. These estimated CIEXYZ Y values were then compared to the TSR-measured CIEXYZ Y values. It was observed that the measurements performed using the TSR were not precise in terms of geometrical conditions (illumination and viewing angles). Also, the measurements used for training the reflection models and to test were generated from the same setup.

Although several image-based setups have been proposed in the past, it is not well established how accurately they perform in comparison to goniospectrophotometers. In this paper, we use the existing image-based measurement setup from [19] and compare the results to two commercially available goniospectrophotometers by transforming the results into a common domain. This is performed for printed packaging paper material samples. We use the terminology "our measurement setup" when referring to the image-based setup from [19]. Second, we investigate the accuracy of the image-based setup by means of a propagation-of-error analysis.

2. METHOD

In this paper, we evaluate the image-based measurement setup used in [19] using commercially available goniospectrophotometer for bidirectional measurements of thin flexible materials. Four material samples (from print and packaging industry) named LightCyan (LC), LightMagenta (LM), Cyan (C) and Magenta (M) are measured using our measurement setup and two commercially available goniospectrophotometers, PerkinElmer's LAMBDA1050, see Appendix A (referred to as LAMBDA1050) and Murakami's GCMS-3B goniospectrophotometric color measurement systems (referred to as GCMS), see Appendix B. To evaluate our measurement setup, we use sample materials printed on matte-coated paper with wax-based inks using an OCE ColorWave600 plotter. Spectralon tile (ST) was measured with LAMBDA1050 and captured with our measurement setup along with the samples. As the samples were solid color patches printed on packaging paper material, they are homogeneous and flexible.

A. Measurements

Out of the four samples, two samples, LC and LM, were measured using LAMBDA1050 while samples C and M were measured using GCMS. The ST was measured using LAMBDA1050 along with LC and LM samples. The appendix

describes both the goniospectrophotometers of their design and measurement output.

For LAMBDA1050, the measurement output is the ratio of reflected radiant flux to incident radiant flux ($\Phi_r/\Phi i$). Radiance factor (β_r) is calculated from the measured output using Eq. (2) [23],

$$\beta_r(\lambda) = \frac{\Phi_r(\lambda)}{\Phi_i(\lambda)} \cdot \frac{\pi}{\omega_r \cos\theta_r}, \tag{2}$$

where ω_r is the detector solid angle, and θ_r is the anormal viewing angle.

The measurement output of GCMS is the radiance factor (β_r). The BRDF can be further calculated using $f_r = \frac{\beta_r}{\pi}$ relation.

Our measurement setup uses a point light source and a commercially available digital camera as a detector. The light source and the detector is at a fixed position from the sample (for example, light source at 45° and detector at 0°), and the measurement sample is curved onto a cylinder of known radius. Figure 1 shows the setup in a vector plane. As described in [19] and referring to Fig. 1, point C is the detector position (digital camera position) approximately at the center of the curved sample at a distance d_C. L is a point light source illuminating the sample at a fixed angle $0° < \theta_L < 90°$ at a known distance d_L from the center of the curved sample. Assuming that the curved sample is homogeneous, light incident, and reflected at any given point on the sample provides information with respect to the light source position (L), camera (C), and surface normal vector (**n**) at point P. θ_i and θ_r are incident and reflection angles with respect to the normal **n** at a given point (P). Considering the setup in a vector plane, θ_i and θ_r are calculated as given in Eq. (3), as follows:

$$\cos\theta_i = \frac{\mathbf{P_L}\cdot\mathbf{n}}{|P_L|}, \qquad \cos\theta_r = \frac{\mathbf{P_C}\cdot\mathbf{n}}{|P_C|}. \tag{3}$$

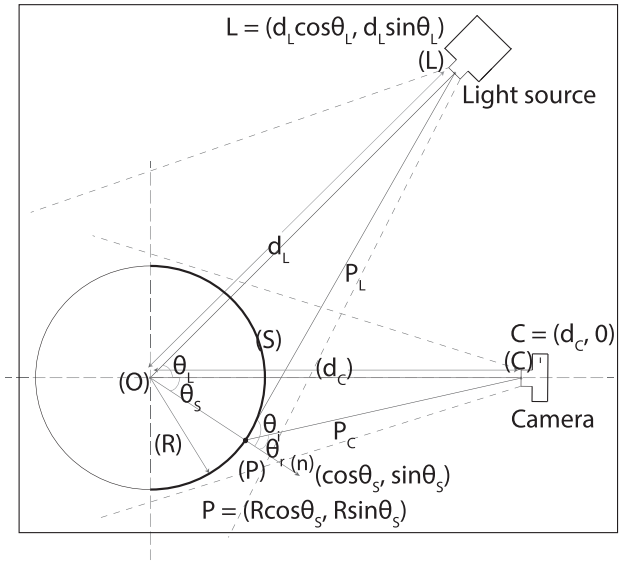

Fig. 1. Measurement setup in a vector plane (Reprinted with permission of IS&T: The Society for Imaging Science and Technology, sole copyright owners of CIC22: Twenty-second Color and Imaging Conference) [19].

As the measurements are performed using a digital camera, each pixel in the captured image corresponds to point (P) on the curved sample surface. As each point (P) (on the sample) makes a corresponding incident (θ_i) and reflection (θ_r) angle with respect to the normal (**n**) at point (P), the information recorded by each pixel corresponds to a bidirectional measurement at point (P).

As discussed in [22], the captured image records the light information in digital values for each camera sensor. The measured camera spectral sensitivities ($r(\lambda)$, $g(\lambda)$, $b(\lambda)$) along with CIE 2° color matching functions ($\overline{x}$, $\overline{y}$, $\overline{z}$) are used to calculate a 3×3 matrix, $\hat{M}$. Using $\hat{M}$, the captured RGB data can be converted into a colorimetric space (CIEXYZ).

Samples LC, LM, and ST, were measured at three anormal incident ($\theta_i = 25°, 35°, 45°$) and 26 anormal reflection angles (ranging between $\theta_r = [+75°, -75°]$ at 5° intervals) using LAMBDA1050. A ratio of the reflected radiant flux to incident flux (Φ_r/Φ_i) in the range of 380 nm to 730 nm at 10 nm intervals was recorded. We calculate the radiance factor using Eq. (2). The distance between the sample and the detector was 91 mm, while the detector aperture area was 12.7 mm× 15.5 mm, thus giving a solid angle (ω_r) of 0.0237 sr [24].

Similarly, samples C and M were measured using GCMS. Spectral radiance factor is recorded in the range of 390 nm to 730 nm at 10 nm interval at anormal incident (θ_i) and reflection (θ_r) angles in the range of [+80°, −80°] at 5° intervals.

In our measurement setup, the sample is illuminated using a tungsten point light source, and was captured using a 16 bit Nikon D200 DSLR camera. As a point light source we use a film projector (consisting of a halogen tungsten lamp). As the projector uses a focusing lens, using the inverse square law we calculate the origin of the point light source by illuminating a white patch at two distance intervals and measure the illuminated area of the white patch and distance between the projector and the illuminated surface. Figure 2 shows a schematic diagram of the setup and measurements. Referring to Fig. 2, distance x is calculated as 103.2 cm. The homogeneity of the light source was checked by measuring the incident light at different parts of the given sample area. The incident beam was homogeneous with a variation of approximately 7.2% across an area of size 5 cm × 2.5 cm at the sample surface.

As a white reference, ST is used in the setup. Illumination and viewing angles are calculated for each pixel point (p) that corresponds to the given point (P) on the curved sample. As discussed in [19], for a given illumination direction (θ_L), the number of viewing directions that we can measure will depend on the sample curvature, resolution of the digital camera used as detector, and the distance between the curved sample and the detector. Also, as we measure the curved sample at different illumination directions (θ_L), the area illuminated on the curved sample changes with change in θ_L. It is therefore important to consider the viewing angles in the area, which is uniformly illuminated with all the illumination directions for further processing and comparison.

LC and LM samples were measured at three different illumination directions ($\theta_L = 24.5°$, 31.5°, and 37°) using our measurement setup (refer Fig. 3). Figure 3 shows the image captured at $\theta_L = 24.5°$. C and M samples were measured at

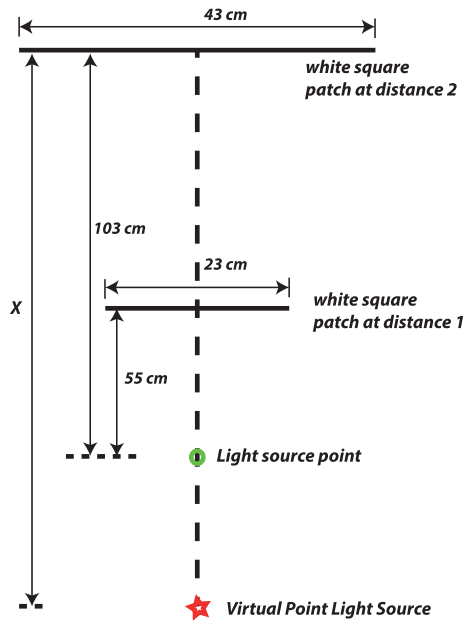

Fig. 2. Virtual point light source calculation.

seven different illumination directions [$\theta_L = 15°$, 18°, 20°, 25°, 28°, 30°, and 35° (refer Fig. 4)]. Figure 4 shows the image captured at $\theta_L = 15°$. As can be seen from the image along with these two samples, five additional samples were measured using our measurement setup; however, it was not possible to

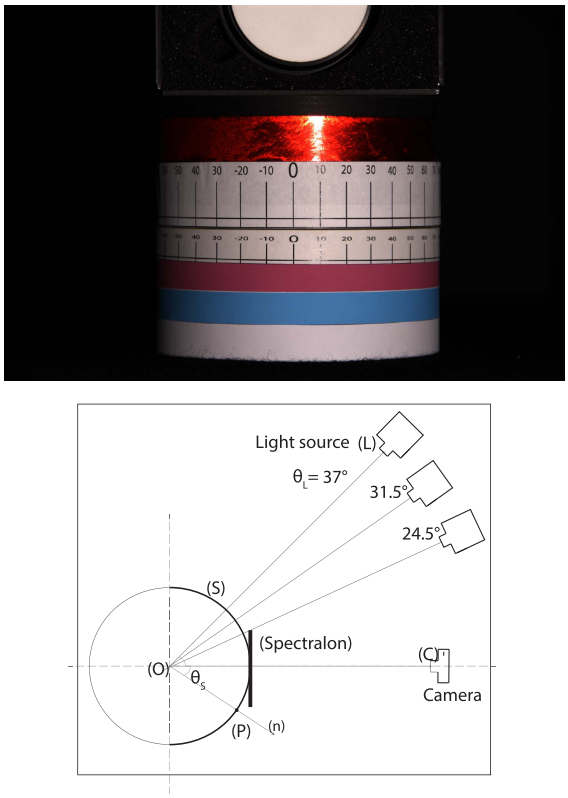

Fig. 3. LC and LM sample measurement at three different illumination directions (θ_L) and image captured at $\theta_L = 24.5°$.

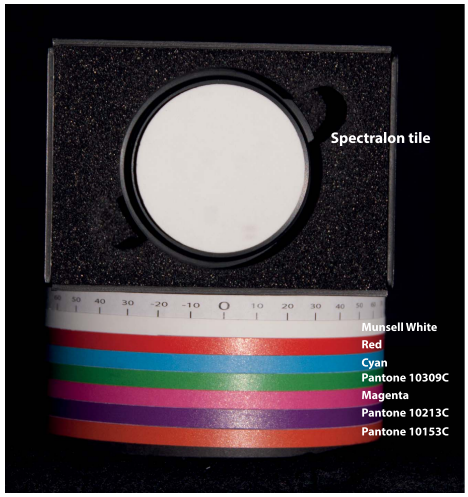

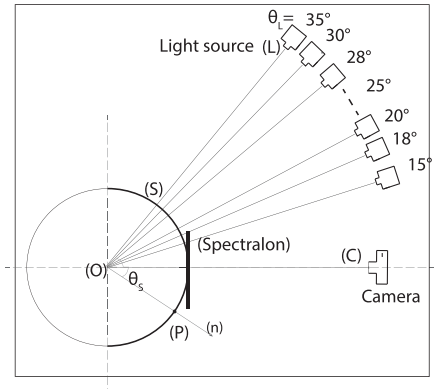

Fig. 4. Sample measurement at seven different illumination directions (θ_L) and image captured at $\theta_L = 15°$.

have them measured using any of the goniospectrophotometers. We therefore use two samples (M and C) in the analysis and comparison. Figure 5 gives an overview of the measurement angles and the instruments with which the samples were measured. Figures 6 and 7 show θ_i and θ_r angles at which the samples were measured using both the goniospectrophotometers and our measurement setup. Please make a note that the GCMS goniospectrophotometer measures at 1° near specular angles while at 5° intervals away from the specular direction.

The camera records a 16 bit raw RGB image. To correct for dark current noise we subtract a dark image (captured with the camera lens cap on in a dark room) from the captured image. Five vertical pixels from the sample center for the given point

Measurement Device	Data Recorded	Samples Measured				
		ST	LC	LM	C	M
Measurement Setup	*Camera RGB*	*3 + 7 direc* (θ_L)	*3 direc* (θ_L = 24.5°, 31.5°, 37°)		*7 direc* (θ_L = 15°, 18°, 20°, 25°, 28°, 30°, 35°)	
LAMBDA1050	*Spectral BRDF*	θ_i = 25°, 35°, 45°			-NM-	
		θ_r = [−75°, +75°] *at* 5° *interval*				
GCSM		-NM-			$\theta_i = \theta_r$ = [−80°, +80°] *at* 5° *interval*	
-NM- = Could not be measured						

Fig. 5. Overview of measurement angles and sample measurement.

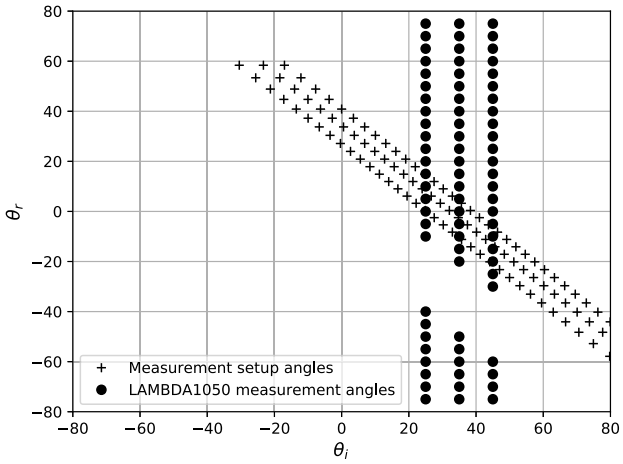

Fig. 6. θ_i and θ_r angles at which LAMBDA1050 and our measurement setup measured.

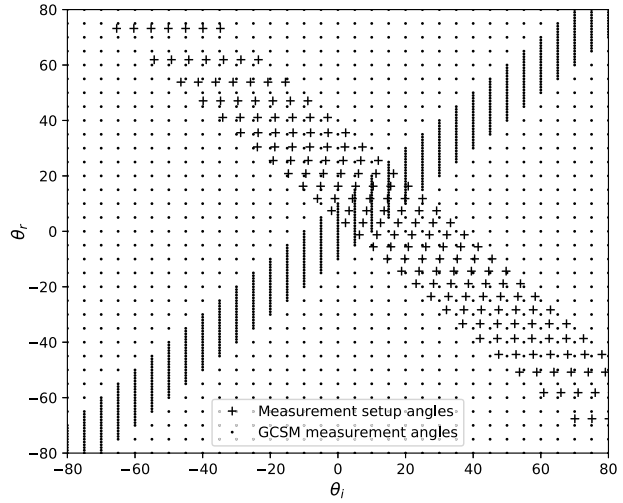

Fig. 7. θ_i and θ_r angles at which GCMS and our measurement setup measured.

(P) are averaged. Camera settings have been similar while measuring the camera spectral sensitivities and while measuring the samples.

In radiometric terms, the 16 bit raw RGB data recorded corresponds to the radiance exited from the curved sample surface (as we work at a constant exposure time, the RGB data recorded corresponds to radiance). To compare the measurements made using our measurement setup and goniospectrophotometers, we need to either calculate the spectral radiance factor from the raw RGB data measurements, or vice versa.

Using the BRDF definition, the radiance exited from the sample surface can be calculated using the sample BRDF measured by the goniospectrophotometer. For a small homogeneous area, spectral radiance reflected from the sample surface in a given direction can be defined as given in Eq. (4),

$$L_r(\theta_i, \phi_i, \theta_r, \phi_r, \lambda) = f_r(\theta_i, \phi_i, \theta_r, \phi_r, \lambda) \cdot E_i((\theta_i, \phi_i, \lambda), \quad \textbf{(4)}$$

where $L_r(\theta_i, \phi_i, \theta_r, \phi_r, \lambda)$ is the spectral radiance exited from the sample, E_i $((\theta_i, \phi_i, \lambda)$ is the spectral irradiance at the sample, and f_r is the sample BRDF (obtained from the goniospectrophotometer measurements). Considering inplane measurements, we rewrite Eq. (4) using the inverse square law as

$$L_r(\theta_i, \theta_r, \lambda) = f_r(\theta_i, \theta_r, \lambda) \cdot \frac{I_i(\lambda) \cdot \cos\theta_i}{\omega_s \cdot d^2}, \quad \textbf{(5)}$$

where $L_r(\theta_i, \theta_r, \lambda)$ and $f_r(\theta_i, \theta_r, \lambda)$ are as described above in Eq. (4) for inplane measurements, $I_i(\lambda)$ is radiant intensity incident normally on the sample, θ_i is anormal incident angle made by the light source relative to the normal at the sample surface, d is distance between sample surface and point light source, and ω_s is the solid angle at the curved sample surface made by the incident light.

In Eq. (5), $f_r(\theta_i, \theta_r, \lambda)$ can be measured using a goniospectrophotometer. The incident spectral light intensity, $I_i(\lambda)$ (in our measurement setup), can be calculated using a reference white diffuser such as a ST whose BRDF is known for a given θ_i and θ_r, and assuming that this reference white diffuser is Lambertian. Distance d will be the distance between point (P) on the curved sample and the point light source in our measurement setup. ω_s will be the solid angle, defined as the ratio of illuminated surface area and square of the distance between the curved surface and light source. We calculate these terms as described below.

Incident spectral light intensity, $I_i(\lambda)$, is estimated using the relative normalization method [25]. The ST BRDF measured with LAMBDA1050 at $\theta_i = 25°$ and $\theta_r = 0°$ is used for the same. Rewriting Eq. (5), incident spectral light intensity can be calculated using Eq. (6),

$$I_i(\lambda) = \frac{L_{r,\text{spec}(\theta_i=25°,\theta_r=0°,\lambda=380\text{ nm–}730\text{ nm})} \cdot d^2}{f_{r,\text{spec}(\theta_i=25°,\theta_r=0°,\lambda=380\text{ nm–}730\text{ nm})} \cdot \cos\theta_i}, \quad \textbf{(6)}$$

where $L_{r,\text{spec}}(\theta_{i=25°}, \theta_{r=0°}, \lambda_{380\text{ nm–}730\text{ nm}})$ is the spectral radiance exited from the spectralon surface and $f_{r,\text{spec}}(\theta_{i=25°}, \theta_{r=0°}, \lambda_{380\text{ nm–}730\text{ nm}})$ is the spectral BRDF of the spectralon measured with LAMBDA1050, at the given incident ($\theta_{i=25°}$) and reflection ($\theta_{r=0°}$) angle. θ_i and d are the same as defined in Eq. (5).

The *distance* (d) is the distance P_L in our measurement setup vector space (refer Fig. 1). d can therefore be calculated using the coordinate values for point P on the curved sample surface and point light source L. We solve for distance P_L [refer Eq. (7)] where d_L is the distance between point light source (L) and origin (O), R is the radius of the cylinder on which the sample is curved, θ_L is the illumination direction angle, and θ_S is the angle made by point (P) on the curved sample surface with vector **OC**, as follows:

$$\mathbf{P}_L = [P, D]\mathbf{P}_L = |P_L| = \sqrt{d_L^2 + R^2 - 2d_L R\cos(\theta_L - \theta_S)}. \quad \textbf{(7)}$$

The *solid angle*, ω_s, can be calculated using the illuminated area and distance between the illuminated sample area and the light source. The distance between the illuminated sample area and the light source is calculated using Eq. (7) at each point (P) on the curved sample surface. As we use a film projector to

illuminate the curved sample, the area illuminated by the point light source will correspond to the physical area on the curved surface covered by each camera pixel.

To calculate the physical area covered by each pixel on the curved sample surface, we ignore errors due to lens structure in the camera and assume that each pixel of the camera makes same solid angle (ω_r) with respect to the captured image and the pixel location on the camera sensor. We capture an image of a white patch with the camera that is used in our measurement setup. Assuming the image of the white patch as a single pixel, the solid angle ω_r formed by the camera with respect to the area of the white patch is as given in Eq. (8). A_{sq} is the physical area of the white patch (in millimeters) and d is the distance between the camera and the white surface (in millimeters), as follows:

$$\omega_r = \frac{A_{\text{sq}}}{d^2} = \frac{(20 \times 25)}{490^2} = 0.00208 \text{ sr.} \tag{8}$$

Dividing the solid angle with the total number of pixels gives us the solid angle (ω_{r_p}) for each pixel. As distance P_L is known for each point (P) on the curved sample surface, ω_s can be calculated using the surface area covered under each pixel. ω_s remained constant over the pixel position (corresponding to the point P on the sample surface) and therefore was taken into account while calculating $I_i(\lambda)$.

Referring to the vector space in Fig. 1, distance P_C between the detector and the sample surface is calculated using Eq. (9). Note that P_C will change with the location on the sample surface as it is curved due to wrapping around a cylinder of radius R,

$$\mathbf{P}_C = [P, C]\mathbf{P}_C = |P_C| = \sqrt{d_c^2 + R^2 - 2Rd_c \cos\theta_s}, \tag{9}$$

where d_C is the distance between the camera (C) and origin (O), R is the radius of the cylinder on which the sample is curved, and θ_S is the angle made by point (P) on the curved sample surface with vector **OC**. As we now know the distance between the camera and the sample surface and the solid angle each camera pixel makes, the physical area covered by each pixel can be calculated using the relation (Area $= \omega \cdot \text{distance}^2$).

To compare the measurements, for simplicity of calculations we convert the sample BRDF to camera RGB values. Referring to Eq. (4), we use the irradiance at the sample surface in our measurement setup to calculate the radiance at the sample surface for the incident (θ_i) and reflection (θ_r) directions at which the sample BRDF is measured using a gonio-spectrophotometer. The light incident on the sample surface, $I_i(\lambda)$, is calculated using Eq. (6). The spectralon BRDF $f_{r,\text{spec}}(\theta_{i=25^\circ}, \theta_{r=0^\circ}, \lambda_{400\text{–}700})$ is measured using LAMBDA1050 while the spectralon surface radiance $L_{r,\text{spec}}(\theta_{i=25^\circ}, \theta_{r=0^\circ}, \lambda_{400\text{–}700})$ is measured using a telespectroradiometer (TSR) in our measurement setup. The camera is replaced by the TSR in our measurement setup to measure the radiance. As the remaining parameters of Eq. (5) are known, we can calculate radiance at the sample surface.

As we compare measurements made using two methods, one being radiance L_r, a physical quantity, while the other is camera RGB, a relative value, the measured data should be calibrated to the incident light intensity in the setup. We scale the incident light intensity using a camera coefficient g as given in Eq. (10). $L_{r,\text{spec}}$ is the radiance measured at the spectralon surface at $\theta_{i=25^\circ}, \theta_{r=0^\circ}, \lambda_{400\text{–}700}$ by replacing the camera with a TSR in our measurement setup, while $\bar{g}(\lambda)$ is the spectral sensitivity of the camera green sensor, as follows:

$$g = \sum_{\lambda=400}^{700\text{ nm}} \bar{g}(\lambda) \cdot L_{r,\text{spec}}(\lambda)\Delta\lambda_{10\text{ nm}}. \tag{10}$$

Using the BRDF measurements of the sample (measured using a goniospectrophotometer), and the scaled incident light intensity ($I_i(\lambda)/g$), the radiance at the sample surface (for the incident (θ_i) and reflection (θ_r) angles at which the BRDF is measured) is calculated using Eq. (11), as follows:

$$L_r(\theta_i, \theta_r, \lambda) = f_r(\theta_i, \theta_r, \lambda) \cdot \frac{I_i(\lambda)}{g} \cdot \frac{\cos\theta_i}{\omega_s \cdot d^2}. \tag{11}$$

The radiance obtained is then converted to camera RGB values using Eq. (12), where $L_r(\theta_i, \theta_r, \lambda)$ is the radiance at the sample surface in our measurement setup calculated using Eq. (11) (but for the incident and reflection angles used in goniospectrophotometer measurements), and ($\bar{r}$, $\bar{g}$, $\bar{b}$) are spectral sensitivities of the camera used as a detector in our measurement setup, as follows:

$$\begin{pmatrix} \text{Cal}_R(\theta_i, \theta_r) \\ \text{Cal}_G(\theta_i, \theta_r) \\ \text{Cal}_B(\theta_i, \theta_r) \end{pmatrix} = \begin{pmatrix} \sum L_r(\theta_i, \theta_r, \lambda) \cdot \bar{r} \\ \sum L_r(\theta_i, \theta_r, \lambda) \cdot \bar{g} \\ \sum L_r(\theta_i, \theta_r, \lambda) \cdot \bar{b} \end{pmatrix}. \tag{12}$$

A point to note here is that when measuring the sample material using a goniospectrophotometer, measurements are performed at fixed incidence (θ_i) and reflection (θ_r) angles, while the measurement setup uses a camera, thus capturing the reflected radiance from the sample surface per pixel. In our measurement setup, each pixel corresponds to the point (P) on the curved sample surface that makes a unique incident (θ_i) and reflection (θ_r) angle relative to the surface normal. Using a high-resolution camera, the θ_i and θ_r combination is high and different compared to the goniospectrophotometer measurements. It records approx. 1000 pixels (horizontally) for each sample.

Another point to note here is that total number of pixels will vary depending upon the radius of the cylinder on which the sample is curved, the distance between the sample and the camera, and the resolution of the camera used in our measurement setup. This data, therefore, being too dense, we use information captured at every 50th pixel for comparison. Depending on the sample material being measured and the interval between the angles required, the pixel interval can be increased or decreased.

We interpolate camera RGB measurements that are calculated using goniospectrophotometer measurements using Eq. (12) at the incident and reflection angles of our measurement setup. Interpolation is performed using a standard piecewise cubic spline interpolation.

B. Measurement Error

Measurement setup has three main components: a camera (as a detector), a point light source (to illuminate the sample), and the sample to be measured (wrapped around a cylinder of known radius). We calculate the incident and reflection angle made by point (P) on the sample with respect to the light direction and the camera position from the curved sample. The incident and reflection angle calculations are therefore

dependent on θ_L (light direction with respect to normal to the camera), cylinder radius (R) on which the sample is wrapped, distance (d_L) between curved sample and point light source, distance (d_c) between curved sample and camera, pixel position (d_p) on the camera with respect to point P on the curved sample surface, and effective camera focal length (F_p). Also, our measurement setup uses a RGB camera as a detector. The camera used in the setup (Nikon D200) records raw RGB data for the radiance exited from the sample surface. We convert this data to CIE XYZ values using a conversion matrix ($\hat{M}$). As discussed in [22], $\hat{M}$ is derived using camera sensitivity measured with a monochromator and CIE 2° color matching functions. Figure 8 shows the sensitivites (measured using the monochromator) of the camera used in our measurement setup. Calculating CIEXYZ values with $\hat{M}$ introduces error in the colorimetric values. It is therefore important to take into account the uncertainty (in terms of measurement error) in these calculations when comparing them to the goniospectrophotometer measurements.

We derive error uncertainty in calculating incident (θ_i) and reflection (θ_r) angles using the procedure given by the Joint Committee for Guides in Metrology (JCGM) [26], as follows:

$$\Delta\theta_{S_{\text{edge}}} = \sqrt{\left(\frac{\partial\theta_{S_{\text{edge}}}}{\partial d_C}\cdot\Delta d_C\right)^2 + \left(\frac{\partial\theta_{S_{\text{edge}}}}{\partial R}\cdot\Delta R\right)^2}$$

$$\frac{\partial\theta_{S_{\text{edge}}}}{\partial d_C} = \frac{-1}{\sqrt{\left(1-\left(\frac{d_C}{R}^2\right)\right)}}\cdot\frac{1}{R}$$

$$\frac{\partial\theta_{S_{\text{edge}}}}{\partial R} = \sqrt{\left[\frac{-\Delta d_C}{R\cdot\sqrt{1-\left(\frac{d_C}{R}\right)^2}}\right]^2 + \left[\frac{d_C\cdot\Delta R}{R^2\cdot\sqrt{1-\left(\frac{d_C}{R}\right)^2}}\right]^2}. \quad \textbf{(13)}$$

Equation (13) shows the uncertainty in calculating $\theta_{S_{\text{edge}}}$. Calculations of $\theta_{S_{\text{edge}}}$ can be referred to in [19]. $\theta_{S_{\text{edge}}}$ is the θ_S angle at the edge of the curved sample when viewed from the camera field of view. In the same way, uncertainty in θ_i, θ_r, θ_S, and F_P is derived and is approximated for the physical measurements Δd_L, Δd_C, $\Delta\theta_S$, ΔR, and $\Delta\theta_L$. Equation (14) calculates the error in CIE Y calculation using values that are calculated using

- $\hat{M}$ and RGB values calculated using Eq. (12) and,
- L_r calculated using Eq. (11) and CIE 2° color matching functions,

$$\Delta Y = \frac{\sqrt{\left(Y_{(\hat{M}\text{-RGB})} - Y_{(L_r\text{-CIE2°})}\right)^2}}{Y_{(L_r\text{-CIE2°})}}. \quad \textbf{(14)}$$

The two samples LC and LM, and the ST were measured using LAMBDA1050 at three anormal incident ($\theta_i = 25°, 35°, 45°$) and 26 anormal reflection angles (ranging between $\theta_r = [+75°, -75°]$ at 5° intervals) while two samples C and M were measured using GCMS in the range of $\theta_i = \theta_r = [+80°, -80°]$ at 5° intervals. All the samples were measured using our measurement setup at different incident light directions (θ_L).

We interpolate measurements conducted with the goniospectrophotometer at angles (θ_i and θ_r) measured at by our measurement setup. A point to note is that the measurements we interpolate here are camera RGB values converted [using Eq. (12)] from the BRDF measurements performed by the goniospectrophotometers. CIEXYZ values were further calculated from the interpolated RGB measurements using the conversion matrix ($\hat{M}$). The ST measurements at $\theta_L = 25°$ were used as reference white measurement with the CIE Y value as 1.0.

To evaluate the setup we analyze the calculated CIE Y value (hereby referred as luminance value). Relative ΔY error is calculated for each sample between the goniospectrophotometer and measurement setup measurements using Eq. (15),

$$\text{Error}_{\Delta Y} = \frac{\sqrt{\left(Y_{\text{Gonio}} - Y_{\text{Setup}}\right)^2}}{Y_{\text{Gonio}}}, \quad \textbf{(15)}$$

where Y_{Gonio} is the luminance value calculated using measurements performed by the goniospectrophotometer and Y_{Setup} is the luminance value calculated using the measurements from our measurement setup of the respective sample material.

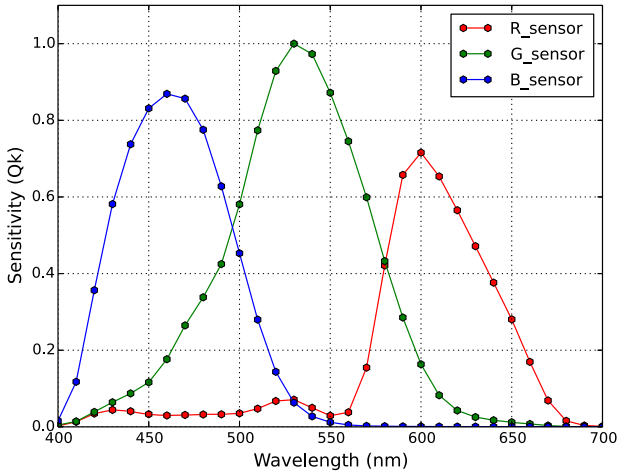

Fig. 8. Camera sensor sensitivity functions (Reprinted with permission of IS&T: The Society for Imaging Science and Technology, sole copyright owners of Electronic Imaging: Measuring, Modeling, and Reproducing Material Appearance 2016) [22].

3. RESULTS

Table 1 shows the uncertainty derived and approximated for our measurement setup parameters. Table 2 shows the uncertainty in CIE Y calculations.

The average $\text{Error}_{\Delta Y}$ for each sample material is calculated (refer Table 3). Figures 9–12 show the calculated luminance for the samples against the reflection angles at the respective incident light direction along with the measurement uncertainty in calculating the angles and CIE Y values. Note that as the number of incident light directions (θ_L) used and samples measured are many when comparing them to GCMS measurements, we show results for the measured samples at one incident direction ($\theta_L = 35°$). For comparison with LAMBDA1050 measurements we show results for both the samples (LC, LM) for one incident light direction ($\theta_L = 44°$).

Looking at the plots we can observe that the measurements performed using the goniospectrophotometers lie within a

Table 1. Measurement Uncertainty in Our Measurement Setup Parameters

	Setup Parameters	Uncertainty
Calculated	θ_i	±7.6°
	θ_r	±7.4°
	θ_S	±6.7°
	F_P	±1973 pixels
Approximated	R	±5 mm
	d_C	±10 mm
	d_P	±5 pixels
	d_L	±20 mm
	θ_L	±4°

Table 2. Error (ΔY) in CIE Y Calculation

Sample	LC	LM	C	M
ΔY	0.11	0.12	0.18	0.13

Table 3. Error$_\Delta$ Y Between Luminance Calculated Using Measurements from Our Measurement Setup and Goniospectrophotometer

Instrument	θ_L	LC Sample	LM Sample
LAMBDA1050	24°	0.12	0.01
	34°	0.14	0.01
	44°	0.18	0.15
	Average	0.14	0.05
Instrument	θ_L	**C Sample**	**M Sample**
GCMS	15°	0.21	0.19
	18°	0.21	0.19
	20°	0.21	0.20
	25°	0.22	0.21
	28°	0.24	0.22
	30°	0.27	0.22
	35°	0.32	0.29
	Average	0.24	0.21

known uncertainty of our measurement setup for the samples used in this study.

4. DISCUSSION

Samples LM and LC were measured at three incident angles (θ_i) using LAMBDA1050 and three light directions (θ_L) in our measurement setup. Owing to measurement setup limitations and the limited measurements from LAMBDA1050, the measurement region of overlap in terms of θ_i and θ_r were limited (refer to Fig. 6). It was therefore possible to compare only a limited number of measurements for the LC and LM samples. A point to note here is that we perform a relative comparison using BRDF measurement of the ST (at $\theta_i = 25°$, $\theta_r = 0°$) to normalize both the measurements. A similar comparison is done for the C and M samples measured with GCMS. With GCMS, it was possible to measure the entire plane for incident and reflection angles at 5° interval (refer to Fig. 7). The same samples were measured at seven different incident light directions (θ_L) using our measurement setup to have a bigger overlap in the measurement region (with respect to θ_i and θ_r directions) compared to the measurements performed using LAMBDA1050 for LC and LM samples. The average ΔY between the measurements was highest for the C sample compared to other samples. The measurement setup we evaluate in this paper has different components. We calculated the error in incident and reflection angle calculations, and CIEXYZ calculations from the camera RGB.

The error in physical measurements [cylinder radius (R), distance between the curved sample and the detector (d_C), distance between the curved sample and the light source (d_L), and angles between d_C and $d_L(\theta_L)$] contributes to the error in estimating the incident and reflection angles at point (P) on the curved sample surface. The uncertainty in estimating θ_i and θ_r is large. We observed that the uncertainty in calculating θ_i and θ_r angles is more sensitive to physical measurements d_C, d_L, and θ_L compared to the radius (R) of the cylinder.

To calculate colorimetric values we use the conversion matrix ($\hat{M}$) along with camera measurements. $\hat{M}$ is calculated using least square error between the camera sensitivity functions and the CIE 2° color matching functions. Depending on the color of the sample being measured, conversion from camera RGB to CIEXYZ will introduce an error in the colorimetric values due to matrix ($\hat{M}$). We calculated this error by comparing the luminance (CIE Y) values calculated using a) the camera measurements and matrix ($\hat{M}$), and b) radiance values and the color matching functions.

Figures 9–12 show the comparison of measurements using the measurement uncertainty (in the form of error bars) of our measurement setup. An important point to understand from these plots is that as long as the measurements obtained from the goniospectrophotometer are within the uncertainty of our measurement setup, it should be possible to use our measurement setup to perform multiangle BRDF measurements with a known uncertainty to measure materials similar to the sample material used in this study. Another point to consider is that we

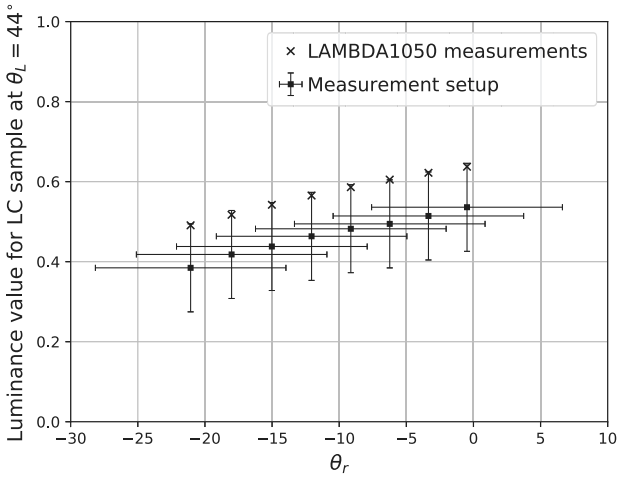

Fig. 9. Calculated luminance (Y) values for LC sample for measurements at $\theta_L = 44°$, using our measurement setup and LAMBDA1050 against θ_r.

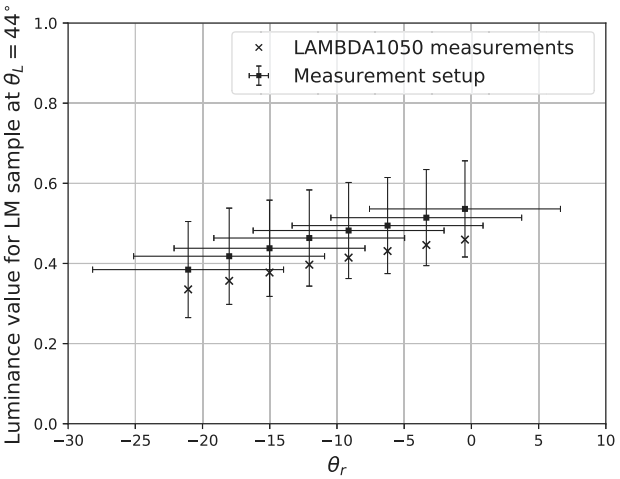

Fig. 10. Calculated luminance (Y) values for LM sample for measurements at $\theta_L = 44°$, using our measurement setup and LAMBDA1050 against θ_r.

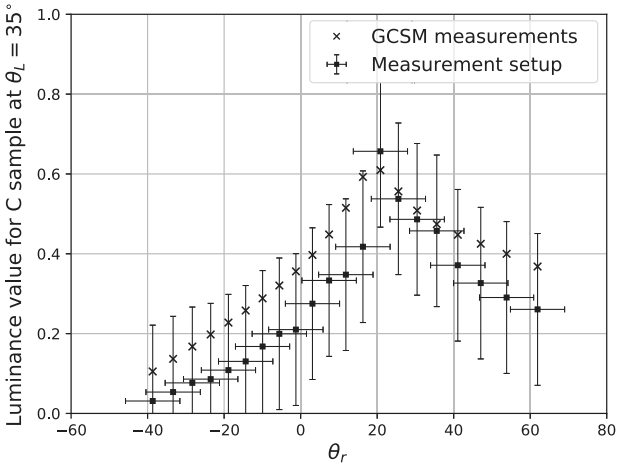

Fig. 11. Calculated luminance (Y) values for C sample for measurements at $\theta_L = 35°$, using our measurement setup and GSCM against θ_r.

have not taken into account the measurement uncertainty of the goniospectrophotometers used in this study. Measurement uncertainty provided by the manufacturer of these instruments is usually for one incident and reflection angle and for one wavelength interval (for example $\theta_i = 45°$, $\theta_r = 0°$, $\lambda = 560$ nm). To calculate the instrument uncertainty with the aim to compare it to the camera setup, it would require a number of approximations to be made that would then add to the comparison error that would be difficult to eliminate. Also, it is expected that the goniospectrophotometers are much more accurate compared to our setup and therefore the uncertainty of our setup, is calculated and analyzed.

Looking at the results obtained for the samples used, luminance (CIE Y) measured using the goniospectrophotometer lies within the measurement uncertainty of our measurement setup. For the LC sample measured at $\theta_L = 44°$, the error is maximum. Although similar observation can be made for C

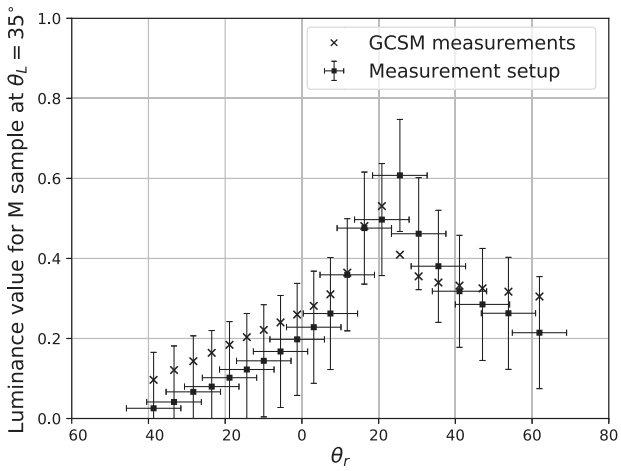

Fig. 12. Calculated luminance (Y) values for M sample for measurements at $\theta_L = 35°$, using our measurement setup and GSCM against θ_r.

sample, the measurements are well within our measurement setup uncertainty. The possible reason for having a large error in the C samples is the camera sensor limitations in the blue spectrum. It is also observed that, as the incident light direction (θ_L) increases, we observe an increase in the error value between the measurements especially for LC and C samples but also for LM and M samples. Increasing θ_L contributes to the error due to geometrical calibration and uncertainty in physical measurements of the setup. Also, the sample being curved, the bigger the θ_L, the more the incident and reflection directions there are for given point P on the sample surface.

From the plots (Figs. 9–12) we can observe that the measurements performed using our measurement setup show lower CIE Y values compared to goniospectrophotometer measurements for LC and C samples. However, for the LM sample our measurement setup measures a higher CIE Y compared to the goniospectrophotometer measurements. For sample M, the measurements from our measurement setup and goniospectrophotometer do not follow a systematic curvature as seen for the other samples (LC, C, and LM). The measurement setup measurements show a lower CIE Y value for reflection angles in an approximate range of −40° to 10° and a higher CIE Y value from approximately $\theta_r = 25°$ to 40°.

The possible reason for such a systematic behavior can be the error in calculating CIE Y value from camera RGB values using the conversion matrix $\hat{M}$. $\hat{M}$ is calculated using the camera spectral sensitivities and the CIE 2° color matching functions. In the CIExy Y colorimetric space, the camera sensitivity values will correspond to the points on the locus of the chromaticity diagram. The error in calculating the CIE Y value from camera RGB will therefore depend on the color sample being converted. These points need a thorough investigation and will be future work for the authors.

From the achieved results can we question if this uncertainty is sufficiently low for a practical use of our measurement setup. The practical use will depend on a) the type of material being measured, b) the measurement accuracy required, and c) implications of the performed measurements. Given the

measurement uncertainty, our measurement setup can be used by customers for fast measurements to understand bidirectional material properties and material visualization. With the obtained uncertainty our measurement setup will not be suitable for precise measurements for applications like security, medical, or measurement traceability.

5. CONCLUSIONS

In this paper, we compare an image-based multiangle measurement setup to commercially available tabletop goniospectrophotometers for bidirectional measurements of flexible and homogeneous materials. We measure four samples using our measurement setup and two goniospectrophotometers at different incident and reflection directions.

Measurement setup can perform multiangle BRDF measurements but with a large uncertainty. Goniospectrophotometer measurements lie within the measurement uncertainty of our measurement setup. The uncertainty in calculating θ_i and θ_r is large, and more precise measurements of the physical parameters are required. Measurement setup can be used to measure (with known uncertainty) materials similar to the sample material used in this paper. The setup can be used for fast multiangle measurements, however with a known uncertainty. Owing to fast measurements using the setup, it can also help automate inline multidirectional measurements during reproduction of packaging materials like the ones used in this study.

APPENDIX A: PERKINELMER'S LAMBDA1050 GONIOSPECTROPHOTOMETER

PerkinElmer's LAMBDA1050 goniospectrophotometer contains an automated reflectance/transmittance analyzer (ARTA) accessory from OMT Solutions BV. The sample to be measured is illuminated with a monochromatic light. The light source used is a tungsten halogen light bulb. It is a double-beam instrument, with the reference beam leading directly to the detector, thus measuring the incident radiant flux (Φ_i) in watts. It uses a double holographic grating monochromator to have a monochromatic light from the light beam incident on the sample. The sample is positioned on a rotating stage, and the angle of incidence (measured from the normal to the sample surface) is varied by rotating the sample using a motor. The light reflected from the sample is detected with an integrating sphere detector of diameter 60 mm and consists of a photomultiplier tube as a detector. The detector revolves around the sample and can be positioned at angles relative to normal of the sample surface, except for $\pm 10°$ near the light source. The measurement output of this instrument is the ratio of reflected radiant flux to incident radiant flux. This instrument has been used previously [23] to study the angular variations in reflectance and fluorescence from paper that contain fluorescent whitening agents and fillers. Please refer to PerkinElmer's LAMBDA1050 manual [Lambda 1050 uv/vis/nir spectrophotometer, http://www.perkinelmer.com/product/lambda-1050-uv-vis-nir-spectrophotometer-l1050?searchTerm=L1050&pushBackUrl=?searchName=L1050. Accessed:2017-03-09] for details and specifications of LAMBDA1050.

APPENDIX B: MURAKAMI'S GCMS-3B GONIOSPECTROPHOTOMETRIC COLOR MEASUREMENT SYSTEM

Murakami's GCMS-3B goniospectrophotometric color measurement system also has a double-beam design wherein the radiant flux reflected from the sample material is continuously compared to measurements made on a reference white diffuser plate. The light source is a tungsten halogen light bulb at a fixed position, while the detector (silicon photodiode array) revolves around the sample within the range of anormal angles $\pm 80°$ to the sample plane (when normal to the incident light). The sample to be measured is mounted on a flat plate, which again rotates between anormal angles $\pm 80°$ with respect to the incident light source normal to the sample plane. The light beam is divided into two identical beams using mirrors, lenses, and heat filters to simultaneously illuminate the sample and the white reference plate. The instrument automatically corrects for the variation in intensity and the area of illumination/viewing, due to the rotation of the plate and the detector. The measurement output of this device is the radiance factor (β) measurement. As the reference white plate used in the measurement is assumed as a perfect reflecting diffuser, we can calculate the BRDF of the sample using the $\beta = \pi \cdot f_r$ relation. Please refer to *Murakami's GCMS-3B Goniospectrophotometric Color Measurement System* manual [Gcms-3 goniospectrophotometer system, http://www.aviangroupusa.com/pdf/GCMS3_Des.pdf. Accessed: 2017-03-09] for details and specifications of this instrument.

Funding. Research Council of Norway (MUVApp project, 250293).

Acknowledgment. We would like to thank and acknowledge support of Dr. Reiner Eschbach, Dr. Jean-Baptiste Thomas, and Dr. Giuseppe Claudio Guarnera at the Norwegian Colour and Visual Computing Laboratory in discussions and suggestions regarding the structure of this paper.

REFERENCES

1. C. Eugène, "Measurement of "total visual appearance": a CIE challenge of soft metrology," in *12th IMEKO TC1 and TC7 Joint Symposium on Man, Science and Measurement* (2008), pp. 61–65.
2. G. Pfaff, *Special Effect Pigments: Technical Basics and Applications* (Vincentz Network GmbH & Co KG, 2008).
3. P. Pjanic and R. D. Hersch, "Specular color imaging on a metallic substrate," in *Color and Imaging Conference* (Society for Imaging Science and Technology, 2013), pp. 61–68.
4. C. McCamy, "Observation and measurement of the appearance of metallic materials. Part I. Macro appearance," Color Res. Appl. **21**, 292–304 (1996).
5. A. Takagi, S. Sato, and G. Baba, "Prediction of spectral reflectance factor distribution of color-shift paint finishes," Color Res. Appl. **32**, 378–387 (2007).
6. E. Kirchner and W. Cramer, "Making sense of measurement geometries for multiangle spectrophotometers," Color Res. Appl. **37**, 186–198 (2012).
7. A. Ferrero, A. Rabal, J. Campos, F. Martínez-Verdú, E. Chorro, E. Perales, A. Pons, and M. L. Hernanz, "Spectral BRDF-based determination of proper measurement geometries to characterize color shift of special effect coatings," J. Opt. Soc. Am. A **30**, 206–214 (2013).

8. CIE, “Colorimetry,” CIE15.2 (2004).
9. ASTM, “Standard practise for multiangle color measurement of metal flake pigmented materials,” ASTM-E2194 (2012).
10. ASTM, “Standard practise for multiangle color measurement of interference pigments,” ASTM-E2539 (2012).
11. C. McCamy, “Observation and measurement of the appearance of metallic materials. Part II. Micro appearance,” Color Res. Appl. **23**, 362–373 (1998).
12. ASTM, “Standard practice for specifying the geometry of multiangle spectrophotometers,” ASTM-E2175 (2013).
13. K. Kehren, “Optical properties and visual appearance of printed special effect colors,” Ph.D. thesis (Technischen Universität Darmstadt, 2013).
14. J. Palmer and B. G. Grant, *The Art of Radiometry* (SPIE, 2010).
15. F. E. Nicodemus, J. Richmond, J. J. Hsia, I. W. Ginsberg, and T. Limperis, *Geometrical Considerations and Nomenclature for Reflectance* (National Bureau of Standards, 1977).
16. CIE, “A framework for the measurement of visual appearance,” Technical Report CIE175 (International Commission on Illumination, 2006).
17. S. Tominaga and N. Tanaka, “Estimating reflection parameters from a single color image,” IEEE Comput. Graph. Appl. **20**, 58–66 (2000).
18. D. Guarnera, G. Guarnera, A. Ghosh, C. Denk, and M. Glencross, “BRDF representation and acquisition,” Comput. Graph. Forum **35**, 625–650 (2016).
19. A. Sole, I. Farup, and S. Tominaga, “An image based multiangle method for estimating reflection geometries of flexible objects,” in *Color Imaging Conference* (2014), Vol. **2014**, pp. 91–96.
20. A. S. Sole, I. Farup, and S. Tominaga, “An image-based multidirectional reflectance measurement setup for flexible objects,” Proc. SPIE **9398**, 93980J (2015).
21. A. Sole, I. Farup, and P. Nussbaum, “Evaluating an image based multiangle measurement setup using different reflection models,” Electron. Imaging **2017**, 101–107 (2017).
22. A. Sole, I. Farup, and S. Tominaga, “Image based reflectance measurement based on camera spectral sensitivities,” Electron. Imaging **2016**, 1–8 (2016).
23. N. Johansson and M. Andersson, “Angular variations of reflectance and fluorescence from paper-the influence of fluorescent whitening agents and fillers,” in *Color and Imaging Conference* (Society for Imaging Science and Technology, 2012), Vol. **2012**, pp. 236–241.
24. N. Johansson, M. Neuman, M. Andersson, and P. Edström, “Influence of finite-sized detection solid angle on bidirectional reflectance distribution function measurements,” Appl. Opt. **53**, 1212–1220 (2014).
25. H. Li, S.-C. Foo, K. E. Torrance, and S. H. Westin, “Automated three-axis gonioreflectometer for computer graphics applications,” Opt. Eng. **45**, 043605 (2006).
26. JCGM, “Evaluation of measurement data—guide to the expression of uncertainty in measurement,” JCGM 100:2008, First edition 100 (2008).